

Comparative study of fracture mechanical test methods for concrete

Lennart Østergaard & John Forbes Olesen

*Department of Civil Engineering, Technical University of Denmark
Brovej, Building 118, DK-2800 Kgs. Lyngby, Denmark.*

ABSTRACT: This paper describes and compares three different fracture mechanical test methods; the uniaxial tension test (UTT), the three point bending test (TPBT) and the wedge splitting test (WST). Potentials and problems with the test methods will be described with regard to the experiment and the interpretation, i.e. the analysis needed to extract the stress-crack opening relationship, the fracture energy etc. Experiments are carried out with each test configuration using mature, high performance concrete. The results show that the UTT is a highly complicated test, which only under very well controlled circumstances will yield the true fracture mechanical properties. It is also shown that both the three point bending test and the WST are well-suited substitutes for the uniaxial tension test.

Keywords: Stress-crack opening relationship, fictitious crack model, forward analysis, inverse analysis, wedge splitting test, three point bending test, uniaxial tension test

1 INTRODUCTION

Concrete exhibits quasi-brittle failure and proper modeling of the initiation and propagation of cracks thus requires knowledge of the stress-crack opening relationship as defined in the cohesive crack model by Hillerborg et al. (1976). This σ - w relationship is often simplified to be bilinear and defined by:

$$\frac{\sigma(w)}{f_t} = \begin{cases} b_1 - a_1 w & 0 \leq w < w_1 \\ b_2 - a_2 w & w_1 \leq w \leq w_2 \end{cases} \quad (1)$$

where w is the crack opening, f_t is the tensile strength, a_1 and a_2 the slopes of the relationship, $b_1 = 1$ and b_2 the normalized ordinate intersection values. Determination of the σ - w relationship for concrete often relies on the use of indirect methods, i.e. methods where a more or less accurate interpretation must be applied in order to extract the needed values. This is the case if e.g. the TPBT is used to determine not only the fracture energy, but also the tensile strength and the σ - w relationship. Also the WST is an indirect method wherefrom the tensile strength and the σ - w relationship may be derived. These methods may be referred to as indirect since the tests yield a load-deformation curve from which

the fracture mechanical properties must be obtained.

The reason for the use of the indirect test methods is the numerous problems related to the UTT. These stem from troubles with achieving a sufficiently stiff testing machine, a sufficiently stiff concrete specimen, ensuring non-rotating end platens and joining end platens to the concrete specimen. It turns out that if the testing machine stiffness or the specimen stiffness is too low, the true fracture mechanical properties related to the descending branch of the load-deformation curve will not be derived, and instead due to stability phenomena, an apparent curve will be obtained, see e.g. Hillerborg (1989) and Østergaard (2003).

The advantages of the indirect test methods are the reduced demands with regard to testing machine and specimen stiffness. If the TPBT is controlled with a constant rate of opening of the crack mouth, very stable experiments may be achieved. Regarding the WST, a stable test may be obtained in most situations applying a constant rate of displacement of the testing machine crosshead, thus enabling practically all testing laboratories the possibility of conducting fracture mechanical testing. The cost, however, when resolving to the indirect methods, is the problems with interpreting the re-

sults. The analysis needed is often termed inverse analysis since here a global load-deformation curve is used as basis for the extraction of the cohesive crack properties through an optimization process. One problem is distinguishing the energy needed to propagate the crack from the energy dissipated elsewhere in the system. Another problem is the analysis itself since local minima may lead to a false σ - w relationship; see e.g. Ulfkjær & Brincker (1993).

However, nowadays the main problems with the inverse analysis seem to be overcome. Wittmann et al. (1987) proposed a method for inverse analysis based on the finite element method, Nanakorn & Horii (1996) devised a method for stepwise multi-linear determination and recently, Østergaard (2003) formulated a method based on the cracked hinge model by Olesen (2001).

The purpose of this paper is to demonstrate the validity of the inverse analysis method by Østergaard (2003) if applied to the TPBT or the WST. This will be achieved by comparing experimental results from the two test configurations with results obtained from the uniaxial tension test. A second objective is to compare results from different experimental geometries and observe how the results obtained from the indirect methods fit the UTT test results. In the paper, the test methods and the methods of analysis will briefly be described where after the experimental results are presented.

2 FRACTURE MECHANICAL TESTING

2.1 The uniaxial tension test (UTT)

The UTT is one of the few test methods, which through a simple interpretation directly yields the σ - w relationship for the material being investigated.

This, however, only holds true if the test is conducted under very well controlled conditions, a fact which has resulted in some debate in the literature. The key issue in the controversy is the influence on the experimental result of the actual propagation of the crack through the specimen, and how this propagation is influenced by rotations at the specimen boundary. Some researchers believe that the specimen boundary should be free to rotate, see e.g. van Mier (1997). In contrast, other researchers believe that not only the specimen boundary but also more important the material in the vicinity of the crack, i.e. the crack planes, must be prevented from rotating, see e.g. Hillerborg (1989) and RILEM (2001). The influence of the rotational stiffness of the testing machine was investigated recently by Østergaard (2003) using a full three-dimensional finite element analysis and it was concluded that

the rotational stiffness must be high in order to achieve the true σ - w relationship from the experiment.

2.1.1 UTT experimental setup

The standard RILEM UTT specimen has been adopted in this project, see e.g. RILEM (2001). The specimen is short with a length equal to the diameter of the unnotched specimen ($D = L = 150$ mm, notch depth $a_0 = 15$ mm). The notch is sawn in the mature specimen in order to eliminate any boundary effects from casting a notch. Furthermore, the specimen is sawn from the central part of samples twice the length of the final specimen. It is hereby achieved that any possible boundary effects in the mould at the ends are eliminated. The sawing is conducted with utmost care ensuring that the specimen is undamaged and such that the saw cuts are perpendicular to the specimen axis.



Figure 1. Experimental setup for the UTT.

Figure 1 shows the experimental setup. The specimen is glued unto two steel end platens as shown. The first glued connection is established outside the testing machine in a special arrangement ensuring a good alignment. The second gluing is conducted in the testing machine such that no redundant loads are imposed on the specimen. A stiff connection between the testing machine and the specimen is achieved by prestressing the wedges. A machine stiffness of 251 kNm/rad has been established. Note also the measurement rig shown in Figure 1.

2.1.2 Interpretation and inverse analysis of UTT

The extraction of the σ - w relationship based on the result from the UTT is easily conducted by simply calculating the stress from the force and by subtracting the elastic contribution to the deformation:

$$w = u_{avg}(\sigma) - u_{avg}(\sigma_{max}) + \frac{\sigma_{max} - \sigma}{K_i} \quad (2)$$

in which K_i is the initial flexibility of the specimen over the measuring distance, u_{avg} is the average displacement at the stress σ and $u_{avg}(\sigma_{max})$ is the average displacement at peak stress, σ_{max} . Note that the peak load will be slightly reduced by the notch effect, however, as shown by Østergaard (2003) the influence is below 5%.

2.2 The three point bending test (TPBT)

The TPBT is widely used for the determination of fracture mechanical properties; especially fracture energy, but also the σ - w relationship. A standard for determination of the fracture energy of concrete has been issued by RILEM (2001). Papers addressing the issue of inverse analysis based on the TPBT have been published; see e.g. Wittmann et al. (1987). The problem has also been addressed by Østergaard (2003).



Figure 2. Experimental setup for the TPBT.

2.2.1 TPBT experimental setup

The experimental TPBT setup is shown in Figure 2. The beam corresponds to the RILEM TPBT beam with a clear span of 500 mm, and a 150x150 mm² cross-section. The supports are able to rotate about an axis parallel to the beam axis and perpendicular to the beam axis. Only the loading device mounted in the crosshead is built-in. A notch with a depth of $a_0 = 25$ mm is cut at mid-span.

A rig is mounted on the beam from which the deflection is measured. This rig is used in order to

exclude false deflection due to deformation of supports etc. The rig is mounted on the centerline of the beam axis just above the supports. Also CMOD is measured during the experiment. This signal is furthermore used as the control signal for the closed loop testing of the beam. The CMOD is measured by mounting two small steel pieces on each side of the notch. An Instron clip-gage is used for the measurements.

2.2.2 Interpretation and inverse analysis of TPBT

The proposed interpretation and inverse analysis of the TPBT is explained in detail in Østergaard (2003). Here, only a brief description of the method will be given.

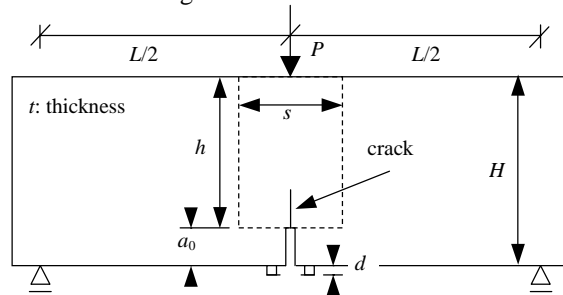


Figure 3. Principal drawing of the TPBT.

Figure 3 shows the principal experimental setup. The clear span is denoted by L , the full height by H , while the beam thickness is denoted by t . The initial notch length is given by a_0 . The CMOD is measured by mounting a clip gage between two measurement points, which are glued onto the beam. These are steel pieces with a height of d .

The analysis is conducted using the cracked hinge model developed by Olesen (2001). Figure 3 shows how the hinge element is implemented in the beam (shown with the dashed lines). The mathematical formulation of the hinge element is given in the referred paper. It is inserted above the initial notch with a height $h = H - a_0$. The width of the hinge is given by s . From investigations, Østergaard (2003), s is expected to be in the order of $H/2$. It is assumed that no axial forces are imposed on the beam, such that $N = 0$. The moment load M is given by:

$$M = \frac{1}{4}PL + \frac{1}{8}mgL \quad (3)$$

where P is the load. Self-weight is included in the expression and the mass is denoted by m and gravity by g . Applying the fact that cracking initiates when the tensile strength f_t is reached in the bottom of the notch (disregarding any stress concentrations) leads to the following expression for the load P_0 at which cracking initiates:

$$P_0 = \frac{2}{3} \frac{t}{L} f_t h^2 - \frac{1}{2} mg \quad (4)$$

The CMOD depends on three different contributions, i.e. the elastic opening, the opening due to formation of the crack, and the geometric amplification due to the notch and the measurement pieces. The elastic deformation of the specimen, just outside the notch, results in an opening, Tada et al. (1985)

$$CMOD_e = \frac{6PLa_0}{EtH^2} v_1 \left(\frac{a_0}{H} \right) \quad (5)$$

in which:

$$v_1(x) = 0.76 - 2.28x + 3.87x^2 - 2.04x^3 + \frac{0.66}{(1-x)^2} \quad (6)$$

The contribution of the small measurement pieces is significant and must be taken into account. According to Karihaloo (1991), this may be done by simply replacing the beam height in Equation 6 by $H = H + d$ and the initial notch length by $a_0 = a_0 + d$. However, Stang (2000) made the assumption that the crack sides are straight, which opens up for a straightforward geometrical correction of Equation 6, $v_1 = (a_0 + d) / a_0 v_1$. FE calculations on the RILEM TPBT geometry show, however, that none of these assumptions precisely capture the influence of the measurement pieces. Nonetheless, the investigation has shown that averaging these corrections reproduces the FE calculations very well, Østergaard (2003). The CMOD at the point of loading where cracking initiates, $CMOD_0$ may be determined from Equations 3 and 5.

$$CMOD_0 = 4a_0 \frac{f_t}{E} \left(\frac{h}{H} \right)^2 v_1 - 3 \frac{mg}{E} \frac{La_0}{tH^2} v_1 \quad (7)$$

Two more terms contribute to the total CMOD in the cracked phases. Opening due to the presence of the crack is given by, Olesen (2001)

$$CMOD_c = \frac{sf_t}{E} \frac{1 - b_i + 2\alpha\theta}{1 - \beta_i} \quad (8)$$

in which θ is the normalized rotation $\theta = hE\varphi / (sf_t)$ of the hinge (φ is the rotation), α is the extension of the crack normalized with the ligament height h and b_i and $\beta_i = f_i a_i s / E$ depend on the stage of crack propagation. The opening due to the geometric amplification is given by, Stang (2000)

$$CMOD_g = \frac{2(a_0 + d)sf_t}{hE} (\theta - 1) \quad (9)$$

Similar results are readily obtained for the deflection, i.e. cracking initiates at u_0

$$u_0 = \frac{f_t}{E} L \left(\frac{h}{H} \right)^2 \left(\frac{1}{6} \frac{L}{H} + v_2 \right) - \frac{mg}{Et} \left[\frac{3}{4} \left(\frac{L}{h} \right)^2 v_2 + \frac{1}{8} \left(\frac{L}{H} \right)^3 \right] \quad (10)$$

where E is modulus of elasticity and $v_2(a_0/H)$ is:

$$v_2(x) = \left(\frac{x}{1-x} \right)^2 (5.58 - 19.57x + 36.82x^2 - 34.94x^3 + 12.77x^4) \quad (11)$$

The elastic deflection is given by:

$$u_e = \frac{1}{4} \frac{P}{Et} \left(\frac{L}{H} \right)^2 \left(\frac{L}{H} + 6v_2 \right) \quad (12)$$

while the total deflection is:

$$u = \theta + \left(\frac{L}{3s} \left(\frac{h}{H} \right)^3 + 2 \frac{h}{s} \left(\frac{H}{h} \right)^2 v_2 - 1 \right) \mu(\theta) \quad (13)$$

in which $\mu(\theta) = 6M / (f_t h^2 t)$ is the normalized hinge moment $M(\theta)$. The equations form the basis for interpretation and inverse analysis of the TPBT. The interpretation proceeds by balancing the internal moment with the external. The idea in the inverse analysis is to use a stepwise algorithm, where the optimization problem is solved in steps corresponding to the different phases of crack propagation. First, the optimization is conducted in the elastic phase with the modulus of elasticity as the only free parameter, and only considering the observations belonging to the elastic phase. This first part, named Step I, see Equation 14, will result in a fast and reliable determination of the modulus of elasticity. It is important to realize that the initial guess on the tensile strength will determine how many observations to include in the optimization. But with reasonable initial guesses and by globally re-running the optimization process (including all steps) this is a minor problem, since the global iterations will converge at the true phase change point. Having determined an estimate for the modulus of elasticity, the next step is to formulate an optimization strategy for the cracked phases. It turns out that the best strategy is to separate the problem into two, such that f_i and a_1 are determined first (Step II), while a_2 and b_2 are determined subsequently (Step III). This is due to results showing that local minima may be avoided using this approach. In contrast to Step I, all observations must now be included in the optimization. If only observations belonging to the actual phase (e.g. phase I) were considered, a spurious solution may be found. This solution represents the minimum where the constitutive parameters have been selected such

that no observation belongs to the considered phase. Utilizing all observations in the cracked phases, and using the mean square of differences between observations and predictions as an error norm, the optimization problem reads:

Step I - determination of E

$$\min_E \frac{1}{N_{max}^0} \sum_0^{N_{max}^0} (P_{sp} - \hat{P}_{sp})^2 \quad (14)$$

Step II - determination of f_t and a_1

$$\min_{(f_t, a_1)} \frac{1}{N_{max}} \sum_0^{N_{max}} (P_{sp} - \hat{P}_{sp})^2 \quad (15)$$

Step III - determination of a_2 and b_2

$$\min_{(a_2, b_2)} \frac{1}{N_{max}} \sum_0^{N_{max}} (P_{sp} - \hat{P}_{sp})^2 \quad (16)$$

where N_{max}^0 and N_{max} represent the last observation belonging to phase 0 and the total number of observations, respectively. The optimization is restricted such that only physical meaningful solutions are found ($E > 0$, $f_t > 0$ etc.). More details concerning the inverse analysis and the validation with regard to finite element analysis may be found in Østergaard (2003).

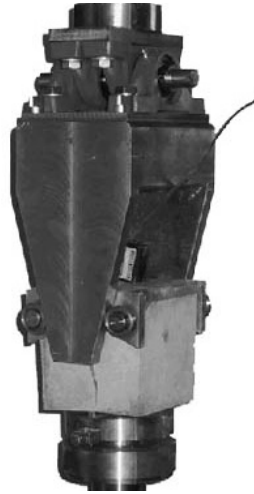


Figure 4. Experimental setup for the WST.

2.3 The wedge splitting test (WST)

The WST is very interesting for many reasons. The idea of this test is to split a small cube with a groove and notch in two halves while monitoring the load and crack mouth opening displacement (CMOD). Originally, this test was designed for determination of the specific fracture energy, G_f , however by application of a suitable model, the σ - w relationship may also be extracted. The test is very stable since the specimen stores very little elastic

energy during testing. Finally, this test method is well suited for inverse analysis.

2.3.1 WST experimental setup

The experimental WST setup is shown in Figure 4. The vertical loading of the wedge and the opening at load line (using a clip gage) are recorded during experiments. Closed loop CMOD control may be used to control the experiment. However, constant rate of displacement of the wedge is often satisfactory since the experiment is very stable.

2.3.2 Interpretation and inverse analysis of WST

The proposed interpretation and inverse analysis of the WST is explained in detail in Østergaard (2003). Here, only a brief description of the method will be given.

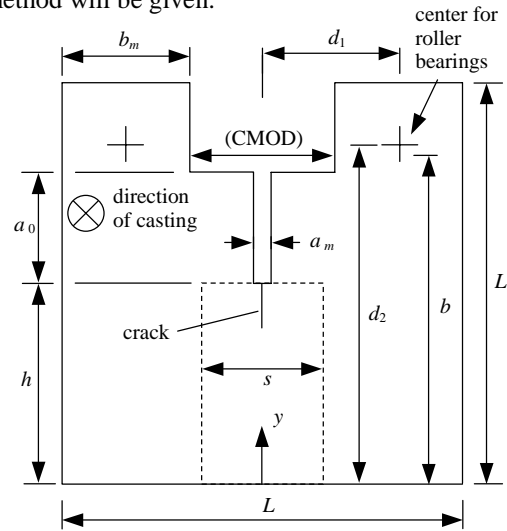


Figure 5. Principal drawing of the WST.

Figure 5 shows the geometry of the WST specimen. The side length of the cube is L and the thickness $t = L$. The initial notch length is a_0 while the ligament length is h . The coordinates of the center of the roller bearings are described by d_1 , which is the horizontal distance from the center-line, and d_2 , the distance from the bottom of the specimen. The CMOD is measured at a distance b from the bottom of the specimen in a cast groove with the width $W = L - 2b_m$. The figure also shows how the hinge element (dashed lines) is incorporated in the specimen with a width of s . The experiment is conducted in compression as illustrated in Figure 4. The compressive load, P_v , is related to the splitting load, P_{sp} , through the expression by Rossi et al. (1991)

$$P_v = \frac{2 \tan \alpha_w + 2\mu_c}{1 - \mu_c \tan \alpha_w} P_{sp} = k P_{sp} \quad (17)$$

where μ_c denotes the coefficient of friction in the roller bearings, while α_w is the wedge angle. According to Rossi et al. (1991), manufacturers of roller bearings give μ_c -values ranging from 0.1% to 0.5%. Ignoring friction in this range generates an error ranging from 0.4% to 1.9% on the splitting load. The sectional forces at the line of symmetry with reference to a distance $h/2$ over the bottom of the specimen may now be calculated:

$$N = P_{sp}$$

$$M = P_{sp} \left(d_2 - \frac{h}{2} \right) + \frac{1}{2} P_v d_1 + \frac{1}{2} m g e \quad (18)$$

where m = mass of specimen and g = gravity. Cracking initiates when the tensile strength is reached in the bottom of the notch. This yields the cracking load P_{sp}^0

$$P_{sp}^0 = \frac{f_t h^2 t - 3 m g e}{6 d_2 + 3 d_1 k - 2 h} \quad (19)$$

in which k is given by Equation 17. The magnitude of the CMOD in the cracked phases is influenced by the same three contributions as in the TPBT setup. These are the elastic opening $CMOD_e$, the opening due to presence of the crack $CMOD_c$ and the amplification caused by the distance from the bottom of the notch to the CMOD-gage, $CMOD_g$. The first term is given by, Tada et al. (1985)

$$CMOD_e = \frac{P_{sp}}{E t} v_2 \quad (20)$$

where $v_2(1-h/b)$ is a function of geometry given by

$$v_2 = \frac{x}{(1-x)^2} (38.2 - 55.4x + 33.0x^2) \quad (21)$$

Note that Equation 21 is only strictly valid for the WST geometry given in Tada et al. (1985). It may, however, be used as an approximation, but the true v_2 value for a certain setup may also be determined on basis of FE analysis. The opening due to the crack, $CMOD_c$, is equal to the expression given in the section on the TPBT setup, see Equation 8. The last contribution, $CMOD_g$ may be shown to be equal to, Østergaard (2003):

$$CMOD_g = 2 (b - h) \left(\frac{CMOD_c}{2\alpha h} - \frac{s f_t}{h E} \frac{\theta_{0-I}}{1 - \beta_1} \right) \quad (22)$$

in which θ_{0-I} is the normalized rotation at crack initiation.

These equations form the basis for the interpretation and inverse analysis of the WST experiment. The procedure is entirely analogous to the method described in the section on the TPBT experiment.

3 EXPERIMENTAL PROCEDURE

Table 1 shows the mix designs used in the experimental investigations. For this study a high performance concrete mix with low water cement ratio and micro silica addition has been investigated.

Table 1. Mix design. The letter P means powder and is given by $P = C + F + SF$. The maximum aggregate size was $d_{max} = 16\text{mm}$. $w/p = 0.307$.

Constituent	Amount
	kg/m ³
Cement (C)	310.0
Fly ash (F) (0.20 C)	62.0
Silica fume (SF) (0.05 C)	15.5
Water	112.8
Air entraining agent (0.001 P)	0.388
Plasticizer (0.006 P)	2.33
Super plasticizer (0.016 P)	6.2
FA, sea gravel, 00-04 mm	783.0
CA, sea gravel, 04-08 mm	343.7
CA, sea gravel, 08-16 mm	687.5

The concrete was mixed using a continuous pan mixer. First, the dry materials were mixed for 2 minutes, then water was added and the mixing continued for another minute before the admixtures were added. Total mixing time was 5 minutes.

WST-specimens were cast in special wooden watertight molds manufactured for this purpose. The groove and the notch in the WST-specimens were cast using tapered PVC inserts. The beams were also cast in wooden watertight molds manufactured for the purpose. The concrete was compacted on a table vibrator for 2 minutes at 50 Hz.

The specimens were covered with plastic and cured in the molds for the first 24 hours. They were then water cured for two months. Thereafter, the specimens were placed in the concrete lab and thus subjected to the (small) temperature variations and drying conditions of the lab. This is probably not the most optimal setting because it may cause drying stress in the specimens, and this stressing will be different from one specimen type to another. However, the effect is probably minimal given that the conditions were maintained for four months before testing. Age at testing was thus 6 months.

The geometry of the WST-specimens is shown on Figure 5. The side length of the fundamental WST-cube is $L = 100$ mm, and the thickness $t = 100$ mm. The height of the ligament is $h = 50$ mm,

while the splitting load is applied at $(d_1, d_2) = (40, 85)$ mm. The length of the notch is $a_0 = 28$ mm, while the mean width of the notch is $a_m = 4.5$ mm. The beams are cast according to the RILEM specifications, RILEM (2001), and the span is 500 mm, while the cross section is 150×150 mm².

A total number of 5 UTT, 5 TPBT and 10 WST were tested. The high number of WST specimen was chosen since it was expected that the scatter on these specimens would be large due to the ligament size vs. maximum aggregate size, i.e. 50 mm vs. 16 mm.

4 RESULTS AND DISCUSSION

The specimen type comparative study aims at comparing results obtained from UTT, WST and TPBT. This comparison will challenge the inverse analysis methods, which have been described briefly in the previous sections. It will furthermore be determined whether the extraction of a specimen independent σ - w relationship is possible.

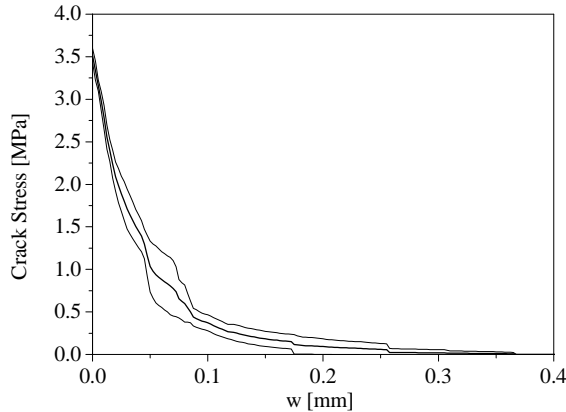


Figure 6. σ - w relationships determined by UTT. The thick line represents the average of all 4 experiments while the thin lines show the standard deviation.

Figure 6 shows the results from the UTT experiments. One experiment has been discarded due to a poor glued connection between the specimen and the steel platen. This gluing has most likely resulted in a significant eccentric loading of the specimen, causing a too low peak load (approx. 2.8 MPa). The glued connection failed shortly after peak load, and after re-gluing a *higher* peak load was determined (approx. 3.0 MPa). Figure 6, therefore, only shows the results from the remaining four experiments.

Three features of Figure 6 are noted. First, the figure demonstrates an increased scatter at a crack stress of approximately 1 MPa. This occurs due to the fact that all the curves show a hump. Thus, de-

spite the effort to give the testing machine a higher rotational stiffness, the stiffness was too low to prevent a hump. The second thing to be noted in Figure 6 is the sudden changes in stress level and scatter at the tail of the curve. This is simply caused by the termination of the individual experiments. Finally, note the very small scatter in determination of tensile strength.

The tensile strength determined from the UTT is assumed to be the true uniaxial tensile strength of the material under investigation, since the notch effect only reduces the peak load by a few percent as noted previously. Thus, in the comparison with the other test methods, this value is fixed and the inverse analysis algorithms for these methods are calibrated using this value. The free parameter in this calibration is the crack bandwidth parameter, s . It turns out that this calibration is necessary in order to arrive at precise results.

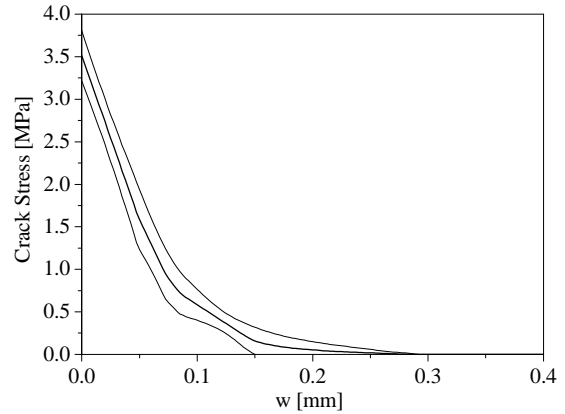


Figure 7. σ - w relationships determined by WST. The thick line represents the average of all 10 experiments while the thin lines show the standard deviation.

Figure 7 shows the σ - w relationships determined using the WST setup. The scatter is, as expected, higher in this experiment than e.g. for the UTT setup, but clearly within acceptable limits. Note that the curves shown in Figure 7 are produced from the bilinear curves determined from the inverse analysis, by averaging the stresses at distinct crack openings, w . The underlying bilinear σ - w curve does of course impose some restrictions on the average curve shown in the figure. It is noted that graphs showing the standard deviation for the TPBT have been omitted from the paper, but the trends are similar to the WST. However, the average TPBT curves are shown in Figure 8 together with the average curves for the UTT and WST. The similarity in the first part of the σ - w relationship between the WST, TPBT-U and TPBT-CMOD results is quite striking. These two indirect experi-

ments do in fact predict the same initial slope for the σ - w relationship. The correlation is not as good for the tail. Here, the highest degree of correlation is found between the WST and the TPBT-U curves, while the TPBT-CMOD curve yields higher values. However, the largest discrepancy is between the UTT and the WST and TPBT curves. The UTT curve is almost without exception below the other curves, indicating lower specific fracture energy of this experiment. Some of the explanation is the hump as discussed earlier in this section, but other factors are also playing a role, including the influence of differences in energy dissipation in the material surrounding the crack in the various tests.

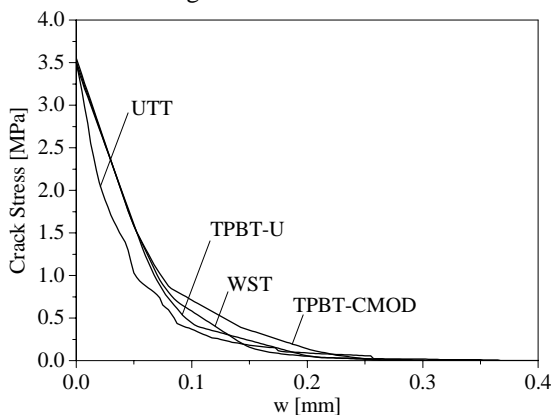


Figure 8. σ - w relationships as determined from the test methods.

Despite the differences seen in Figure 8, there is no doubt that the results show that it is possible to determine practically similar σ - w relationships from different test methods, and that the results obtained from the indirect methods are useful and close to the result which may be obtained from the UTT.

5 CONCLUSIONS

It has been shown that both the TPBT and the WST may be used for the determination of the σ - w relationship for concrete. This is very advantageous since the UTT is much more difficult to perform.

The analytical method known as the cracked hinge model has been applied with success and provides a solid basis for the interpretation of results obtained from the WST and the TPBT. It is thereby unnecessary to use time-consuming finite element methods.

It is, however, noted that an initial calibration of the methods must be conducted since the crack band parameter has an influence on the result. This may be done by e.g. carrying out experiments with both the WST and the TPBT and comparing the results.

6 REFERENCES

- Hillerborg, A., Mod er, M. & Petersson, P. E. 1976. Analysis of crack formation and crack growth in concrete by means of fracture mechanics and finite elements. *Cem Conc Res* 6: 773-782.
- Hillerborg, A. 1989. Stability problems in fracture testing. In *Fracture of Concrete and Rock. Recent Developments*: 369-378. Elsevier Applied Science.
- Karihaloo, B. L. & Nallathambi, P. 1991. Notched beam test: Mode I fracture toughness. In S. Shah & A. Carpinteri (eds.), *Fracture Mechanics Test Methods for Concrete*: 1-86. Chapman & Hall.
- Linsbauer, H. N. & Tschegg, E. K. 1986. Fracture energy determination of concrete with cube shaped specimens (in German). *Zement und Beton* 31: 38-40.
- van Mier, J. G. M. 1997. *Fracture Processes of Concrete*, CRC Press, Boca Raton.
- Nanakorn, P. & Horii, H. 1996. Back analysis of tensioning-softening relationship of concrete. *J Mat Conc Struct Pav* 32(544): 265-275
- Olesen, J. F. 2001. Fictitious crack propagation in fiber-reinforced concrete beams. *J Eng Mech* 127(3): 272-280
- RILEM 2001, Rilem-Committee-TDF-162, Chairlady L. Vandewalle, main author Stang, H., Test and design methods for steel fiber reinforced concrete, recommendations for Uniaxial Tension Test. *Mat & Struc* 34(235): 3-6
- Rossi, P., Br hwiler, E., Chhuy, S., Jenq, Y.-S. & Shah, S. P. 1991. Fracture Properties of Concrete as Determined by Means of Wedge Splitting Tests and Tapered Double Cantilever Beam Tests. In S. Shah & A. Carpinteri (eds.), *Fracture Mechanics Test Methods for Concrete*: 87-128. Chapman & Hall.
- Stang, H. 2000. Analysis of 3 point bending test. Technical Report EU Contract - BRPR-CT98-813. Report from test and design methods for steel fiber reinforced concrete. 7p.
- Tada, H., Paris, P. & Irwin, G. 1985. *The stress analysis of cracks handbook*. Paris Productions Inc., 226 Woodbourne Dr., St. Louis, Missouri, USA.
- Ulfkj r, J. P. & Brincker, R. 1993. Indirect determination of the σ - w relation of HSC through three-point bending. In *Fracture and damage of concrete and rock - FCD-2*: 135-144. E & FN Spon.
- Wittmann, F.H., Roelfstra, P.E., Mihashi, H., Huang, Y.-Y. and Zhang, X.-H. 1987. Influence of age of loading, water-cement ratio and rate of loading on fracture energy of concrete. *Mat and Struc* 20: 103-110.
-  stergaard, L. 2003. *Early-age fracture mechanics and cracking of concrete. Experiments and modeling*. PhD-thesis. Department of Civil Engineering, Technical University of Denmark, Lyngby, Denmark.